A measurement of the $K^+ \to \pi^+\mu^+\mu^-$ decay

The NA62 collaboration

E-mail: na62eb@cern.ch, lubos.bician@cern.ch

ABSTRACT: A sample of 2.8×10^4 $K^+ \to \pi^+\mu^+\mu^-$ candidates with negligible background was collected by the NA62 experiment at the CERN SPS in 2017–2018. The model-independent branching fraction is measured to be $(9.15 \pm 0.08) \times 10^{-8}$, a factor three more precise than previous measurements. The decay form factor is presented as a function of the squared dimuon mass. A measurement of the form factor parameters and their uncertainties is performed using a description based on Chiral Perturbation Theory at $\mathcal{O}(p^6)$.

Contents

Introduction

The flavour-changing neutral current decays $K^{\pm} \to \pi^{\pm}\ell^{+}\ell^{-}$ (denoted $K_{\pi\ell\ell}$), with $\ell = e, \mu$ have been the focus of extensive theoretical work [1–4]. Dominant contributions to the $K_{\pi\ell\ell}$ decays are mediated by virtual photon exchange $K^{\pm} \to \pi^{\pm}\gamma^{*} \to \pi^{\pm}\ell^{+}\ell^{-}$ and involve long-distance hadronic effects described by a vector interaction form factor.

Studies of the $K_{\pi ee}$ and $K_{\pi\mu\mu}$ decay form factors contribute to experimental tests of lepton flavour universality [5, 6]. The first lattice QCD calculation of the form factor value at a specific lepton pair mass (lying outside the $K_{\pi\mu\mu}$ kinematic region) using physical light-quark masses is presented in [7]. Future methodology optimizations together with advances in computing technology are expected to provide competitive lattice QCD predictions of the form factor.

The E787 collaboration at the Brookhaven National Laboratory reported the first observation of the $K_{\pi\mu\mu}$ decay in 1997 [8], which was followed by the E865 [9] and HyperCP [10] measurements. The E865 result established the vector nature of the decay form factor, while HyperCP studied both $K_{\pi\mu\mu}^{+}$ and $K_{\pi\mu\mu}^{-}$ decays and measured the CP violating

decay rate asymmetry, found to be compatible with zero. The most precise study [11] of $K_{\pi\mu\mu}$ was performed by the NA48/2 collaboration at the CERN SPS. The $K_{\pi ee}$ decay was first observed at the CERN PS by the Geneva-Saclay collaboration in 1975 [12], and subsequently measured by the E777 [13], E865 [14] and NA48/2 [15] experiments. A summary of form factor measurements can be found in [16].

Improved measurements of the $K_{\pi\mu\mu}$ model-independent branching fraction and form factor parameters, based on the dataset collected in 2017–2018 by the NA62 experiment at the CERN SPS, are presented in the following. The forward-backward asymmetry of the decay with respect to angle $\theta_{K\mu}$ between the K^+ and the μ^- three-momenta in the $\mu^+\mu^-$ rest frame, is also measured.

1   Beam, detector and data sample

The layout of the NA62 beamline and detector [17] is shown schematically in figure 1. An unseparated secondary beam of π^+ (70%), protons (23%) and K^+ (6%) is created by directing $400\,\mathrm{GeV}/c$ protons extracted from the CERN SPS onto a beryllium target in spills of 3 s effective duration. The target position defines the origin of the NA62 reference system: the beam travels along the Z axis in the positive direction (downstream), the Y axis points vertically up, and the X axis is horizontal and directed to form a right-handed coordinate system. The central beam momentum is $75\,\mathrm{GeV}/c$, with a momentum spread of 1% (rms).

Beam kaons are tagged with a time resolution of 70 ps by a differential Cherenkov counter (KTAG), which uses nitrogen gas at 1.75 bar pressure contained in a 5 m long vessel as radiator. Beam particle positions, momenta and times (to better than 100 ps resolution) are measured by a silicon pixel spectrometer consisting of three stations (GTK1,2,3) and four dipole magnets. A toroidal muon sweeper, called scraper (SCR), is installed between GTK1 and GTK2. A 1.2 m thick steel collimator (COL) with a $76{\times}40\,\mathrm{mm}^2$ central aperture and 1.7×1.8 m^2 outer dimensions is placed upstream of GTK3 to absorb hadrons from upstream K^+ decays; a variable aperture collimator of 0.15×0.15 m^2 outer dimensions was used up to early 2018. Inelastic interactions of beam particles in GTK3 are detected by an array of scintillator hodoscopes (CHANTI). A dipole magnet (TRIM5) providing a $90\,\mathrm{MeV}/c$ horizontal momentum kick is located in front of GTK3. The beam is delivered into a vacuum tank evacuated to a pressure of 10^{-6} mbar, which contains a 75 m long fiducial volume (FV) starting 2.6 m downstream of GTK3. The beam angular spread at the FV entrance is 0.11 mrad (rms) in both horizontal and vertical planes. Downstream of the FV, undecayed beam particles continue their path in vacuum.

Three-momenta of charged particles produced in K^+ decays are measured by a magnetic spectrometer (STRAW) located in the vacuum tank downstream of the FV. The spectrometer consists of four tracking chambers made of straw tubes, and a large aperture dipole magnet (M), located between the second and third chamber, that provides a horizontal momentum kick of $270\,\mathrm{MeV}/c$. The momentum resolution is $\sigma_p/p = (0.30 \oplus 0.005 \cdot p)\%$, with the momentum p expressed in GeV/c.
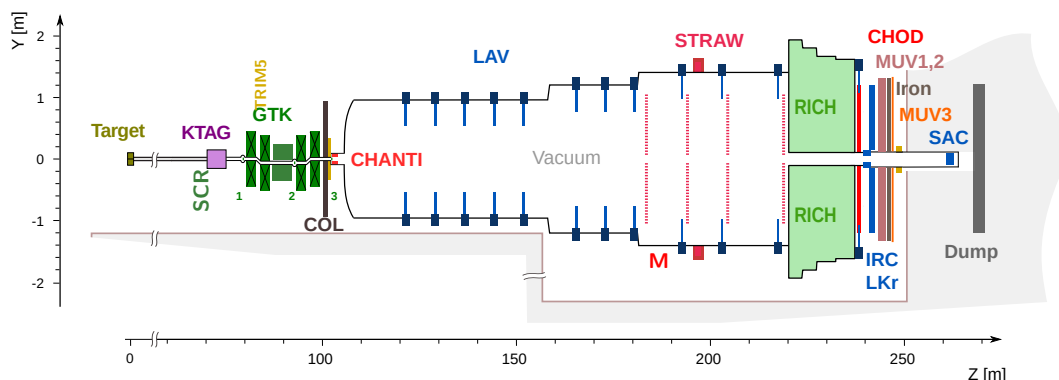
Figure 1. Schematic side view of the NA62 detector.

A ring-imaging Cherenkov detector (RICH) consisting of a 17.5 m long vessel filled with neon at atmospheric pressure (with a Cherenkov threshold of $12.5\,\mathrm{GeV}/c$ for pions) provides particle identification, charged particle time measurements (to a 70 ps accuracy for particles well above the Cherenkov threshold), and the trigger time. Two scintillator hodoscopes (CHOD), which include a matrix of tiles and two planes of slabs arranged in four quadrants located downstream of the RICH, provide trigger signals and time measurements. The tile matrix hodoscope has a time resolution of 1 ns, while the slab hodoscope measures time with 200 ps precision.

A $27X_0$ thick quasi-homogeneous liquid krypton (LKr) electromagnetic calorimeter is used for particle identification and photon detection. The calorimeter has an active volume of 7 m^3 segmented in the transverse direction into 13248 projective cells of 2×2 cm^2 size, and provides an energy resolution $\sigma_E/E = (4.8/\sqrt{E} \oplus 11/E \oplus 0.9)\%$, with E expressed in GeV. To achieve hermetic acceptance for photons emitted in K^+ decays in the FV at angles up to 50 mrad from the beam axis, the LKr calorimeter is supplemented by annular lead glass detectors (LAV) installed in 12 positions inside and downstream of the vacuum tank, and two lead/scintillator sampling calorimeters (IRC, SAC) located close to the beam axis. An iron/scintillator sampling hadronic calorimeter formed of two modules (MUV1,2) and a muon detector consisting of 148 scintillator tiles located behind an 80 cm thick iron wall (MUV3) are used for particle identification. The eight smaller tiles of MUV3 adjacent to the beam pipe are referred to as the *inner tiles*, while the remaining 140 regular tiles are called the *outer tiles*.

The data sample used for this analysis is obtained from 0.84×10^6 SPS spills collected in 2017–2018, with the typical beam intensity increasing over time from 1.5×10^{12} to 2.2×10^{12} protons per spill. The latter value corresponds on average to a 500 MHz instantaneous beam particle rate at the FV entrance, and a 3.7 MHz K^+ decay rate in the FV. The main trigger of NA62 is dedicated to the collection of the very rare $K^+ \to \pi^+\nu\bar\nu$ decays [18]. Multi-track (MT) and di-muon multi-track (2μMT) triggers considered in this analysis operate concurrently, downscaled by typical factors of 100 and 2, respectively. The downscaling factors of both triggers were varied throughout the data taking. The MT trigger line selects the $K^+ \to \pi^+\pi^+\pi^-$ ($K_{3\pi}$) decays, used for normalization, while the

2μMT line selects the $K_{\pi\mu\mu}$ signal decays. The low-level hardware (L0) trigger [19] for both lines is based on RICH signal multiplicity and coincidence of signals in two opposite CHOD quadrants. The 2μMT line additionally involves a requirement of signal coincidence in two outer MUV3 tiles. The high-level software (L1) trigger requires K^+ identification by KTAG, and reconstruction of a negatively charged STRAW track for both MT and 2μMT trigger lines. A detailed description of the NA62 trigger system and its performance is given in [20].

Monte Carlo (MC) simulations of particle interactions with the detector and its response are performed using a software package based on the GEANT4 toolkit [21]. In addition, the accidental activity is simulated, and the response of both trigger lines is emulated.

2 Event selection

Kinematic similarities of the signal ($K_{\pi\mu\mu}$) and normalization ($K_{3\pi}$) decays allow for substantial overlap between the signal and normalization event selections, which results in first-order cancellation of most detector and trigger inefficiencies, thus reducing the systematic uncertainties in the measurement.

The following selection criteria are common to the $K_{\pi\mu\mu}$ and $K_{3\pi}$ event selections.

- Each STRAW track is assigned a time computed as a weighted average of the associated CHOD hodoscope signals. The weights are obtained from the time resolutions of the CHOD hodoscopes. Triplets of STRAW tracks compatible with a common origin in the FV are combined into three-track vertices. Vertex time is defined as the weighted average of the times of CHOD signals associated with the vertex tracks.

- Exactly one three-track vertex with the following properties is required to be present: total charge $q = 1$, time within 6 ns of the trigger time, Z position between 110 m and 180 m from the target, total momentum compatible with the mean beam momentum within $2.5\,\mathrm{GeV}/c$, total transverse momentum with respect to the beam axis below $30\,\mathrm{MeV}/c$, and vertex distance from the beam axis below 5 cm. The beam axis and momentum are monitored throughout the data taking with fully reconstructed $K_{3\pi}$ decays. Only the three tracks forming the chosen vertex are considered in the following.

- All track times must be within 12 ns of the vertex time, and the vertex time is required to be within 6 ns of a KTAG kaon signal.

- The tracks must be within the geometrical acceptance of all STRAW chambers, and extrapolate to lie within the CHOD, LKr, and MUV3 acceptances.

- The track momenta should exceed $10\,\mathrm{GeV}/c$ to ensure track reconstruction efficiency above 90%. The angles between each track and the beam axis must be smaller than 9 mrad to reduce background to the $K_{\pi\mu\mu}$ sample from $K_{3\pi}$ decays followed by $\pi^{\pm} \to \mu^{\pm}\nu$ decays.

- The spatial separation between each pair of vertex tracks must be at least 15 mm in the plane of the first STRAW chamber and 200 mm in the LKr front plane to suppress photon conversions and the overlap of energy deposits.

The following particle identification criteria are employed.

- A track is identified as a charged pion if it has no spatially associated MUV3 signals within 10 ns of the vertex time, and the ratio of the associated LKr cluster energy to the track momentum is $E/p < 0.9$.

- A track with $E/p < 0.2$ is identified as a muon if it has a spatially associated MUV3 signal in an outer tile within 6 ns of both the vertex and the trigger times.

The following criteria are specific to the $K_{\pi\mu\mu}$ event selection.

- Only vertices with tracks identified as $\pi^+ \mu^+ \mu^-$ are considered.

- To reduce the background from $K_{3\pi}$ decays occurring upstream of the FV, the track identified as a π^+ is extrapolated backward to the COL plane, taking into account the TRIM5 magnetic field. The extrapolated position is required to lie outside a rectangle defined by $|X| < 40$ mm and $|Y| < 25$ mm.

- Further $K_{3\pi}$ background suppression is achieved by requiring the momenta of both muon tracks to be below $45\,\text{GeV}/c$.

- The invariant mass $m(\pi\mu\mu)$ of the three selected tracks is reconstructed with a $1.1\,\text{MeV}/c^2$ resolution and must be within $8\,\text{MeV}/c^2$ of the nominal K^+ mass m_K [22].

The following criteria are specific to the $K_{3\pi}$ event selection.

- In order to minimize differences between the signal and normalization selections, only one positive track, chosen at random, is required to be identified as a π^+.

- The identified π^+ track extrapolated to the COL plane must satisfy the same requirements as the π^+ in the $K_{\pi\mu\mu}$ selection.

- The invariant mass $m(3\pi)$ of the three selected tracks is reconstructed with a $0.8\,\text{MeV}/c^2$ resolution and must be within $8\,\text{MeV}/c^2$ of m_K.

For both selections, simulated events are required to be accepted by a set of software algorithms emulating the conditions employed in the online trigger system.

3 Signal and normalization samples

The reconstructed mass spectra of the data and simulated events passing the signal and normalization event selections are shown in figure 2. The selected $K_{3\pi}$ data sample, contaminated by background decays to a negligible level of 10^{-6}, is used together with the simulated $K_{3\pi}$ events with inner bremsstrahlung included [23], to obtain the effective number of kaon decays in the FV

$$N_K = \frac{1}{A_{3\pi} \cdot \mathcal{B}_{3\pi}} \cdot \sum_i \frac{N_{3\pi}^i \cdot D_{\text{MT}}^i}{D_{2\mu\text{MT}}^i} = (3.48 \pm 0.09_{\text{syst}} \pm 0.02_{\text{ext}}) \times 10^{12}, \qquad (3.1)$$
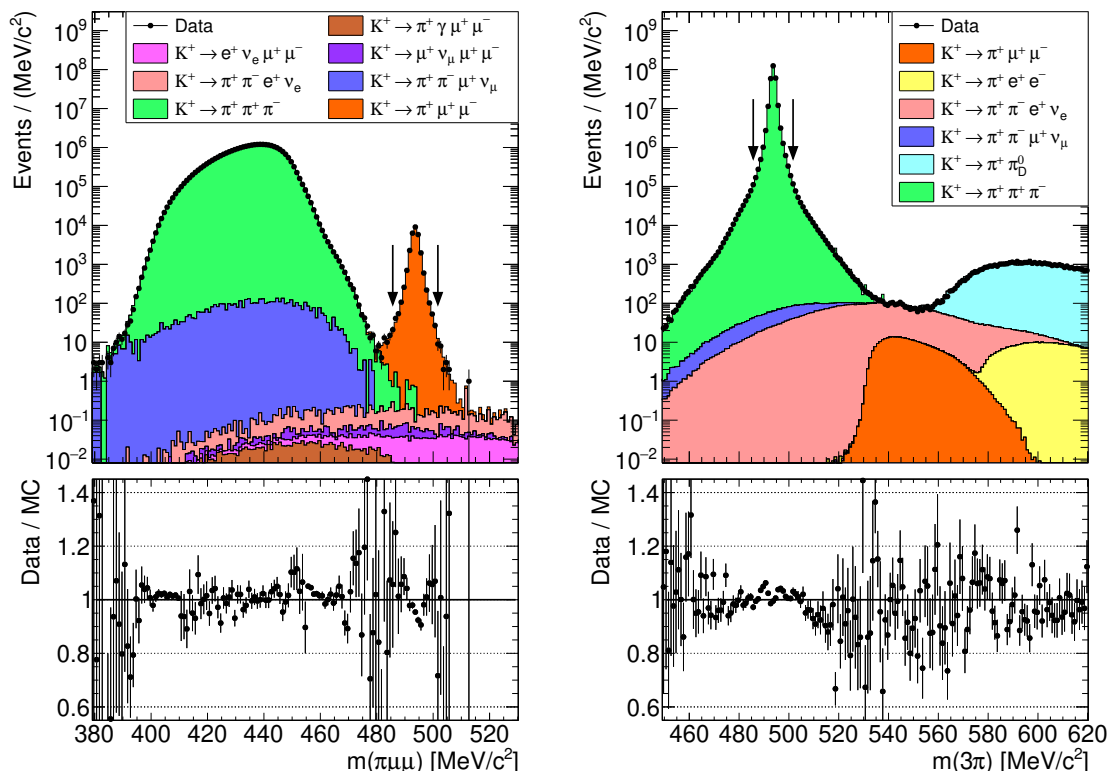
Figure 2. *Top:* reconstructed mass distributions of events satisfying the signal (left) and normalization (right) selections. The arrows indicate the selected mass regions. The contribution from the simulated $K_{\pi\mu\mu}$ decays is scaled according to the PDG branching fraction [22]. *Bottom:* ratios of data and simulated spectra for signal (left) and normalization (right).

where the index i runs over data taking periods defined by constant trigger downscaling factors, $N_{3\pi}^i$ are the numbers of $K_{3\pi}$ events selected with the MT trigger with downscaling factor D_{MT}^i, $D_{2\mu\mathrm{MT}}^i$ are the downscaling factors of the $2\mu\mathrm{MT}$ trigger, and $A_{3\pi} = (6.58 \pm 0.16)\%$ and $\mathcal{B}_{3\pi} = (5.583 \pm 0.024)\%$ are the acceptance (obtained from simulation) and the branching fraction [22] of the $K_{3\pi}$ decay, respectively. The statistical errors in $A_{3\pi}$ and N_K are negligible, while the systematic uncertainties are dominated by the accuracy of the CHOD detector efficiency in the simulation. The external error on N_K stems from the uncertainty on the $K_{3\pi}$ branching fraction.

The $m(\pi\mu\mu)$ signal region contains 27679 data events with a background contamination of about 8 events, estimated from simulation.

4   Interpretation of the data

4.1   Decay width and form factor parameterization

The one-photon-inclusive $K_{\pi\mu\mu}$ differential decay width expressed in terms of the normalized $\mu^+\mu^-$ invariant mass squared $z = m^2(\mu^+\mu^-)/m_K^2$ reads [2–4, 24]

$$\frac{\mathrm{d}\Gamma(z)}{\mathrm{d}z} = \frac{\mathrm{d}\Gamma_{\text{3-body}}(z)}{\mathrm{d}z} + \frac{\mathrm{d}\Gamma_{\text{4-body}}(z)}{\mathrm{d}z} = g(z) \cdot |W(z)|^2 + \frac{\mathrm{d}\Gamma_{\text{4-body}}(z)}{\mathrm{d}z}, \qquad (4.1)$$

where $(2m_\mu/m_K)^2 < z < (1 - m_\pi/m_K)^2$, $W(z)$ is the form factor of the $K^+ \to \pi^+\mu^+\mu^-$ transition, and $g(z)$ is a function describing the decay kinematics [3] and including next-to-leading order electromagnetic effects in terms of radiative corrections. While the $\mu^+\mu^-$ interactions are fully taken into account by virtual and bremsstrahlung corrections for the lepton and meson contributions, discussed in [4] and extended beyond the soft-photon approximation, the semi-classical Coulomb corrections, summarized for example in [25], are applied to the $\pi^+\mu^+$ and $\pi^+\mu^-$ pairs. These last corrections have opposite sign and the same average magnitude; their combined effect on the results of the present analysis is found to be negligible. The hard-photon 4-body ($K^+ \to \pi^+\mu^+\mu^-\gamma$) part of the phase-space is separated from the soft-photon 3-body ($K^+ \to \pi^+\mu^+\mu^-$) part by the condition $(P_\pi + P_\gamma)^2 - m_\pi^2 > 100\,\text{MeV}^2$, where P_π and P_γ are 4-momenta of the π^+ and γ, respectively. The cutoff value is optimized with respect to the experimental resolution. The resulting ratio of the 4-body to 3-body integrated decay widths is $(1.64 \pm 0.02)\%$, where the uncertainty comes mainly from the accuracy of the theoretical description $\mathrm{d}\Gamma_{\text{4-body}}(z)/\mathrm{d}z$ of the 4-body decay [24]. In the present analysis, the 4-body decay width, depending non-trivially on the form factor, is approximated by a unique function displayed in figure 3-left. Effects of this approximation are treated as systematic uncertainties.

The Chiral Perturbation Theory parameterization of $W(z)$ at $\mathcal{O}(p^6)$, introduced in [2], is used in the present paper:

$$W(z) = G_F m_K^2 (a_+ + b_+ z) + W^{\pi\pi}(z), \tag{4.2}$$

where a_+ and b_+ are real parameters, and $W^{\pi\pi}(z)$ is a complex function describing the contribution from a two-pion loop. The term $W^{\pi\pi}(z)$ depends on additional real parameters α_+ and β_+; the values $\alpha_+ = (-20.40 \pm 0.18) \times 10^{-8}$ and $\beta_+ = (-2.05 \pm 0.06) \times 10^{-8}$ [26] are used.

4.2 Measurement of the model-independent branching fraction and form factor

The selected $K_{\pi\mu\mu}$ signal sample with negligible background contamination is distributed in 50 equipopulated bins in z with widths ranging from 0.004 for $z \approx 0.25$ to 0.066 for the last bin. The resolution in z increases linearly from zero to 0.0035 within the allowed kinematic range, and is always several times smaller than the corresponding bin width.

The reconstructed differential decay width, shown in figure 3-left, is given by

$$\left(\frac{\mathrm{d}\Gamma(z)}{\mathrm{d}z}\right)_i = \frac{N_{\pi\mu\mu,i}}{A_{\pi\mu\mu,i}} \cdot \frac{1}{\Delta z_i} \cdot \frac{1}{N_K} \cdot \frac{\hbar}{\tau_K}, \tag{4.3}$$

where for each bin i: $N_{\pi\mu\mu,i}$ is the number of $K_{\pi\mu\mu}$ signal candidates, Δz_i is the bin width, $A_{\pi\mu\mu,i}$ is the signal selection acceptance of the $K_{\pi\mu\mu}$ decay (obtained from simulation, and equal to zero at both kinematic bounds of z while reaching the maximum of 12.5% around $z = 0.2$, see also figure 4-left), N_K is the effective number of kaon decays in the FV collected by the 2μMT trigger (eq. (3.1)), $\hbar$ is the reduced Planck constant, and $\tau_K = (1.238 \pm 0.002) \times 10^{-8}$ s is the mean charged kaon lifetime [22].

The model-independent $K_{\pi\mu\mu}$ branching fraction

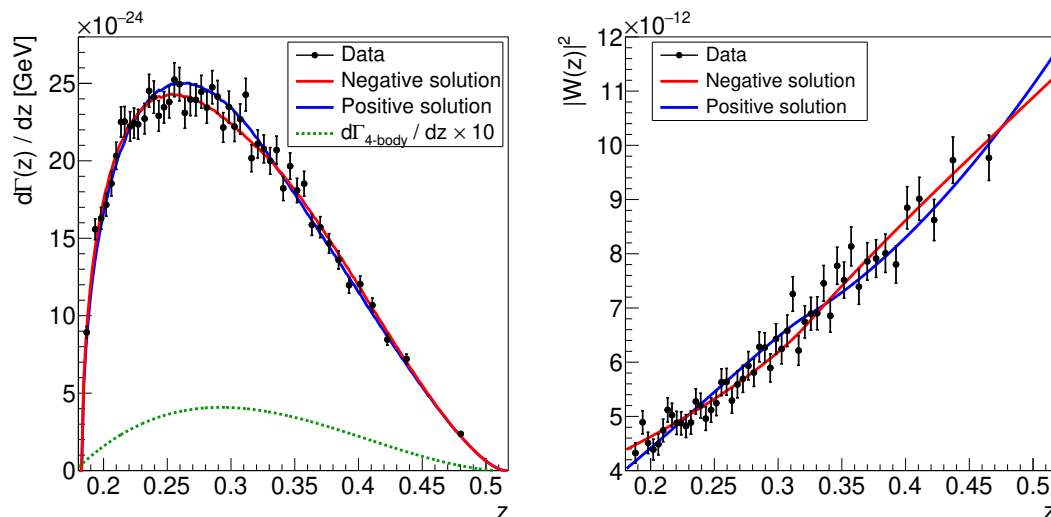$$\mathcal{B}_{\pi\mu\mu} = (9.15 \pm 0.06_{\text{stat}}) \times 10^{-8}$$

Figure 3. *Left:* reconstructed $K_{\pi\mu\mu}$ differential decay width together with the 4-body decay contribution scaled by a factor of 10. The horizontal positions of the data points take into account the non-linearity of the fit function [27]. *Right:* squared modulus of the form factor. The superimposed lines correspond to the two form factor fit solutions defined in the text.
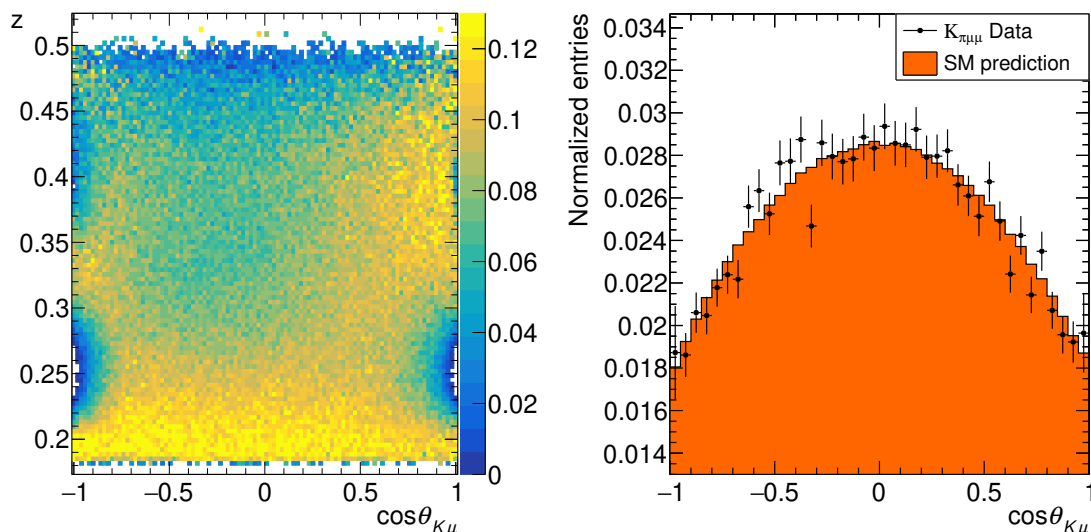

Figure 4. *Left:* signal selection acceptance of the simulated $K_{\pi\mu\mu}$ decays in the $(\cos\theta_{K\mu}, z)$ plane. *Right:* reconstructed $\cos\theta_{K\mu}$ spectrum from data corrected for the acceptance (points with error bars), and the distribution expected from the Standard Model (filled histogram).

is obtained from the reconstructed binned differential decay width (eq. (4.3), figure 3-left) by integrating the spectrum over z and multiplying by $\tau_K/\hbar$.

The $K_{\pi\mu\mu}$ data sample is also used to extract the $|W(z)|^2$ form factor (figure 3-right). The values of the $|W(z)|^2$ function are reconstructed from the differential decay spectrum (figure 3-left) under the assumption that $|W(z)|^2$ is linear in each bin of z. This assumption defines the horizontal positions of the data points in figure 3-right, which are different from the positions in figure 3-left.

The form factor parameters a_+ and b_+ best describing the data are determined by a χ^2 fit of the data points shown in figure 3. Fits of $d\Gamma(z)/dz$ and $|W(z)|^2$ give identical results. The theoretically-preferred [16] *negative solution* with both a_+ and b_+ negative and $\chi^2/\mathrm{ndf} = 45.1/48$ (*p*-value $= 0.59$) is

$$a_+ = -0.575 \pm 0.012_{\mathrm{stat}}, \quad b_+ = -0.722 \pm 0.040_{\mathrm{stat}}, \quad \text{with correlation } \rho(a_+, b_+) = -0.972.$$

A second $\chi^2(a_+, b_+)$ minimum is found, corresponding to the *positive solution*: $\chi^2/\mathrm{ndf} = 56.4/48$ (*p*-value $= 0.19$), $a_+ = 0.373 \pm 0.012_{\mathrm{stat}}$, $b_+ = 2.017 \pm 0.040_{\mathrm{stat}}$, $\rho(a_+, b_+) = -0.973$. Only the negative solution is considered in the following.

4.3 Forward-backward asymmetry measurement

The forward-backward asymmetry A_{FB} of the $K_{\pi\mu\mu}$ decay is defined in terms of the angle $\theta_{K\mu}$ between the K^+ and the μ^- three-momenta in the $\mu^+\mu^-$ rest frame, as

$$A_{\mathrm{FB}} = \frac{\mathcal{N}(\cos\theta_{K\mu} > 0) - \mathcal{N}(\cos\theta_{K\mu} < 0)}{\mathcal{N}(\cos\theta_{K\mu} > 0) + \mathcal{N}(\cos\theta_{K\mu} < 0)}, \tag{4.4}$$

where the numbers of events $\mathcal{N}$ are obtained after correction for the non-uniform acceptance in the $(\cos\theta_{K\mu}, z)$ plane (figure 4-left). The resulting $\cos\theta_{K\mu}$ spectrum of the data events and the distribution expected from the Standard Model (SM) are displayed in figure 4-right.

The asymmetry is measured to be

$$A_{\mathrm{FB}} = (0.0 \pm 0.7_{\mathrm{stat}}) \times 10^{-2}$$

and shows no significant dependence on z. The statistical precision is at the level of the upper limits on A_{FB} predicted by the Minimal Supersymmetric Standard Model [28] and by the calculation of the two-photon intermediate state $K^+ \to \pi^+\gamma^*\gamma^* \to \pi^+\mu^+\mu^-$ [29].

5 Systematic and external uncertainties

The individual contributions to the total uncertainties are discussed in the following and listed in table 1.

5.1 Trigger efficiency

The trigger behaviour is emulated with a set of software algorithms applied to simulated events. The algorithms are tuned and validated on $K_{3\pi}$ events. The L0 RICH, L0 CHOD, L0 MUV3 and L1 KTAG trigger efficiencies (equal to 99.8%, 98.2%, 98.9% and 99.8%, respectively) are found to be independent of the decay kinematics. Data and simulation efficiencies agree within 0.3%. The L1 STRAW trigger efficiency is 94.7% and varies as a function of decay kinematics within $\mathcal{O}(1\%)$. Data and simulation efficiencies agree within 0.5%.

The similarity of the MT and 2μMT trigger lines results in substantial cancellation of trigger-related systematic effects. The residual systematic uncertainties are estimated by either disabling the software trigger emulators in simulation (in the case of the L0 RICH and L0 CHOD conditions), or replacing them with simplified emulators (L0 MUV3, L1 KTAG, L1 STRAW).

5.2 Reconstruction and particle identification

The similarity of the signal and normalization selections allows for significant cancellation of most systematic effects coming from reconstruction and particle identification efficiencies.

Systematic uncertainties arising from differences between event reconstruction efficiencies in data and simulation are dominated by the three-track event reconstruction in the STRAW spectrometer. A dedicated $K_{3\pi}$ event selection, relying on a reconstructed kaon track in the GTK and two pion tracks in the STRAW, is used to measure the efficiency of reconstructing the third pion track. The average measured efficiency is 84% and depends on the decay kinematics. The observed differences of up to 2% between the efficiencies in data and simulation are considered in evaluating the systematic effects resulting from the STRAW track reconstruction efficiency.

The CHOD and MUV3 reconstruction efficiencies are above 99%, with no more than 0.6% difference between data and simulation.

The differences between data and simulation in the hadronic shower development and energy reconstruction in the LKr are another source of systematic uncertainty. No significant difference is observed in the efficiency of the muon identification. The efficiency of the pion identification measured on data is 99%. The agreement between data and simulation varies with pion momentum within 1%. Residual effects due to different $K_{\pi\mu\mu}$ and $K_{3\pi}$ pion kinematics are treated as systematic uncertainties.

5.3 Beam and accidental activity simulation

Systematic uncertainties stemming from the quality of the simulation of the beam momentum spectrum and intensity profile, and from the accuracy of the simulation of the halo muons accompanying the beam, are combined into a single systematic uncertainty. The selected normalization sample of $K_{3\pi}$ events is used for the beam momentum and intensity studies. The halo muons are selected from out-of-time STRAW tracks that have associated signals in MUV3 and are not compatible with originating from decays in the FV.

5.4 Background

The number of background events is estimated using simulation to be 7.8 ± 5.6, where the error comes from the limited statistics of simulated background decays. The background arises mainly from the $K_{3\pi}$ contribution with two $\pi^{\pm} \to \mu^{\pm}\nu$ decays in flight. More details on the methods employed in the $K_{3\pi}$ background estimation can be found in [30].

Systematic uncertainties from the background contamination are estimated conservatively as differences between the results obtained with background neglected and background subtracted.

5.5 External uncertainties

External uncertainties in the measured quantities originate from the $K_{3\pi}$ branching fraction [22], from the accuracy of the radiative corrections to the $K_{\pi\mu\mu}$ decay, including the numerical approximation of $\mathrm{d}\Gamma_{4\text{-body}}/\mathrm{d}z$, and from the pion loop term parameters α_+ and β_+ [26].

	δa_+	δb_+	$\delta\mathcal{B}_{\pi\mu\mu} \times 10^8$	$\delta A_{\mathrm{FB}} \times 10^2$
Statistical uncertainty	0.012	0.040	0.06	0.7
Trigger efficiency	0.002	0.008	0.02	0.1
Reconstruction and particle identification	0.002	0.007	0.02	0.1
Size of the simulated $K_{\pi\mu\mu}$ sample	0.002	0.007	0.01	0.1
Beam and accidental activity simulation	0.001	0.002	0.01	—
Background	0.001	0.001	—	—
Total systematic uncertainty	0.003	0.013	0.03	0.2
$K_{3\pi}$ branching fraction	0.001	0.003	0.04	—
$K_{\pi\mu\mu}$ radiative corrections	0.003	0.009	0.01	0.2
Parameters α_+ and β_+	0.001	0.006	—	—
Total external uncertainty	0.003	0.011	0.04	0.2
Total uncertainty	**0.013**	**0.043**	**0.08**	**0.7**

Table 1. Summary of uncertainties.

6 Comparison with earlier measurements

A comparison of the present results with those from previous measurements by E787, E865, HyperCP and NA48/2 is shown in figure 5, table 2, and table 3.

Note that the NA48/2 measurement [11], until now the most precise, used a different $K_{3\pi}$ branching fraction [31], and did not simulate the inner bremsstrahlung radiation of $K_{3\pi}$ decays. Implementing these conditions in the NA62 analysis has minor impact on the results, which would change by $\delta a_+ = -0.001$, $\delta b_+ = -0.002$, and $\delta\mathcal{B}_{\pi\mu\mu} = +0.03 \times 10^{-8}$.

Furthermore, the analysis by NA48/2 did not simulate inclusive radiative corrections and the 4-body radiative decay $K^+ \to \pi^+\mu^+\mu^-\gamma$ in the $K_{\pi\mu\mu}$ sample, but implemented only the soft-photon Coulomb corrections for all pairs of the $K_{\pi\mu\mu}$ decay products. Adopting this approach changes the NA62 results by $\delta a_+ = -0.006$, $\delta b_+ = +0.034$, and $\delta\mathcal{B}_{\pi\mu\mu} = -0.06 \times 10^{-8}$, where the 0.7% relative change in the branching fraction comes from the increase of the signal acceptance measured with the 3-body simulated $K_{\pi\mu\mu}$ sample including Coulomb corrections.

In addition, previous experiments employed values of $\alpha_+ = -20.6 \times 10^{-8}$ and $\beta_+ = -2.8 \times 10^{-8}$, taken from [2]. Using these values instead of the revised ones ($\alpha_+ = -20.40 \times 10^{-8}$, $\beta_+ = -2.05 \times 10^{-8}$ [26]), the NA62 results would change[1] by $\delta a_+ = -0.011$, $\delta b_+ = +0.026$.

7 Summary

A sample of 27679 $K_{\pi\mu\mu}$ candidates with negligible background contamination was collected by the NA62 experiment in 2017–2018. The size of the $K_{\pi\mu\mu}$ data sample is the main factor limiting the precision of the present analysis.

---

[1]The measured slopes are $\delta a_+/\delta\alpha_+ = +0.004 \times 10^8$, $\delta b_+/\delta\alpha_+ = -0.029 \times 10^8$, $\delta a_+/\delta\beta_+ = +0.013 \times 10^8$, and $\delta b_+/\delta\beta_+ = -0.027 \times 10^8$.
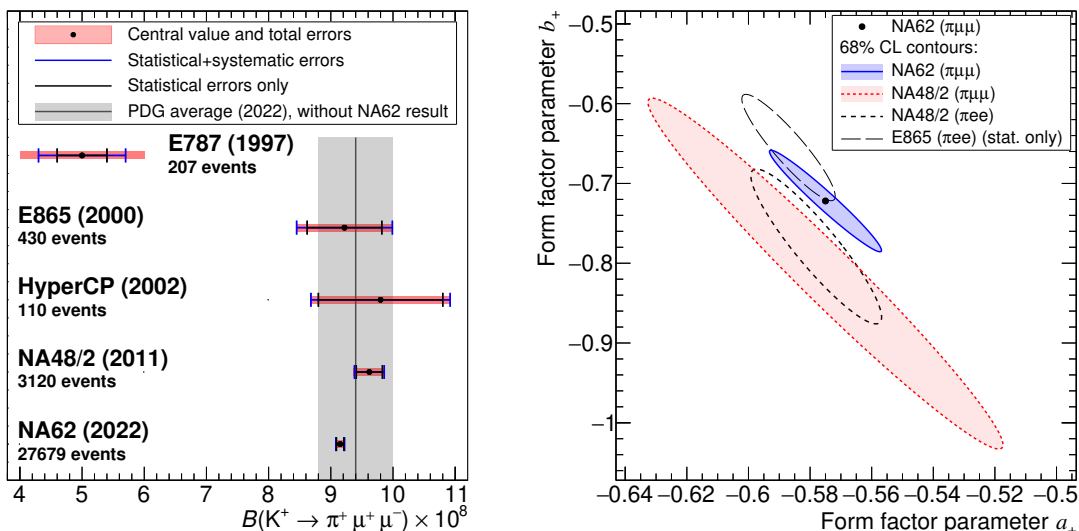
Figure 5. Comparison with earlier measurements. *Left:* the $K_{\pi\mu\mu}$ branching fraction, with the PDG [22] average shown as a shaded band. *Right:* combined statistical and systematic 68% CL contours in the (a_+, b_+) plane for the muon and electron modes. The NA48/2 value of $\rho(a_+, b_+)$ for the electron mode is used to construct the E865 contour, as E865 [14] does not quote the correlation. The systematic uncertainties in a_+ and b_+ are not provided by E865 [14].

Measurement	$K_{\pi\mu\mu}$ candidates	$\mathcal{B}_{\pi\mu\mu} \times 10^8$
E787 [8]	207	$5.0 \ \pm 0.4_{\text{stat}} \ \pm 0.7_{\text{syst}} \ \pm 0.6_{\text{ext}} \ = 5.0 \ \pm 1.0$
E865 [9]	430	$9.22 \pm 0.60_{\text{stat}} \pm 0.49_{\text{syst}} \qquad\quad = 9.22 \pm 0.77$
HyperCP [10]	110	$9.8 \ \pm 1.0_{\text{stat}} \ \pm 0.5_{\text{syst}} \qquad\quad = 9.8 \ \pm 1.1$
NA48/2 [11]	3120	$9.62 \pm 0.21_{\text{stat}} \pm 0.11_{\text{syst}} \pm 0.07_{\text{ext}} = 9.62 \pm 0.25$
NA62, this result	27679	$9.15 \pm 0.06_{\text{stat}} \pm 0.03_{\text{syst}} \pm 0.04_{\text{ext}} = 9.15 \pm 0.08$

Table 2. Comparison with the previous measurements of the $K_{\pi\mu\mu}$ branching fraction.

Measurement	Signal candidates	a_+	b_+	$\rho(a_+, b_+)$
E865, $K_{\pi ee}$ [14]	10300	-0.587 ± 0.010	-0.655 ± 0.044	—
NA48/2, $K_{\pi ee}$ [15]	7253	-0.578 ± 0.016	-0.779 ± 0.066	-0.913
NA48/2, $K_{\pi\mu\mu}$ [11]	3120	-0.575 ± 0.039	-0.813 ± 0.145	-0.976
NA62, $K_{\pi\mu\mu}$, this result	27679	-0.575 ± 0.013	-0.722 ± 0.043	-0.972

Table 3. Comparison with the previous measurements of the $K^\pm \to \pi^\pm \ell^+ \ell^-$ form factor parameters. The E865 $K_{\pi ee}$ measurement [14] does not provide the systematic uncertainties, nor the correlation coefficient of the form factor parameters.

The $K_{\pi\mu\mu}$ model-independent branching fraction is measured to be $(9.15\pm0.08)\times10^{-8}$, consistent with previous measurements and at least a factor of three more precise.

The form factor parameters in the framework of the Chiral Perturbation Theory at $\mathcal{O}(p^6)$ are measured as $a_+ = -0.575 \pm 0.013$, $b_+ = -0.722 \pm 0.043$. Values and statistical

errors of parameters in any other form factor model can be obtained from the reconstructed values of the $|W(z)|^2$ function. The present measurement is the first to employ inclusive radiative corrections in the simulation of the signal channel. The form factor parameters are consistent with those measured by NA48/2, as well as with the results obtained in the electron mode by other experiments, suggesting agreement with lepton flavour universality in the $K_{\pi\ell\ell}$ decays.

The forward-backward asymmetry of the $K_{\pi\mu\mu}$ decay is measured to be $A_{\mathrm{FB}} = (0.0 \pm 0.7) \times 10^{-2}$, a factor of 2.6 improvement in the precision with respect to NA48/2. The experimental precision reaches the level of the upper limits on A_{FB} predicted by the Minimal Supersymmetric Standard Model and by the calculation of the two-photon intermediate state $K^+ \to \pi^+ \gamma^* \gamma^* \to \pi^+ \mu^+ \mu^-$.

References

[1] G. Ecker, A. Pich and E. de Rafael, $K \to pi\ell^+\ell^-$ decays in the effective chiral Lagrangian of the standard model, *Nucl. Phys. B* **291** (1987) 692 [INSPIRE].

[2] G. D'Ambrosio, G. Ecker, G. Isidori and J. Portoles, *The decays $K \to \pi\ell^+\ell^-$ beyond leading order in the chiral expansion*, *JHEP* **08** (1998) 004 [`hep-ph/9808289`] [INSPIRE].

[3] A.Z. Dubnickova, S. Dubnicka, E. Goudzovski, V.N. Pervushin and M. Secansky, *Radiative kaon decay in the chiral perturbation theory*, *Phys. Part. Nucl. Lett.* **5** (2008) 76 [`hep-ph/0611175`] [INSPIRE].

[4] B. Kubis and R. Schmidt, *Radiative corrections in $K \to \pi\ell^+\ell^-$ decays*, *Eur. Phys. J. C* **70** (2010) 219 [`arXiv:1007.1887`] [INSPIRE].

[5] L.C. Tunstall, A. Crivellin, G. D'Ambrosio and M. Hoferichter, *Probing lepton flavour (universality) violation at NA62 and future kaon experiments*, *J. Phys. Conf. Ser.* **800** (2017) 012014 [`arXiv:1611.00495`] [INSPIRE].

[6] G. D'Ambrosio, A.M. Iyer, F. Mahmoudi and S. Neshatpour, *Anatomy of kaon decays and prospects for lepton flavour universality violation*, *JHEP* **09** (2022) 148 [`arXiv:2206.14748`] [INSPIRE].

[7] P.A. Boyle, F. Erben, J.M. Flynn, V. Gülpers, R.C. Hill, R. Hodgson et al., *Simulating rare kaon decays $K^+ \to \pi^+\ell^+\ell^-$ using domain wall lattice QCD with physical light quark masses*, [`arXiv:2202.08795`] [INSPIRE].

[8] E787 collaboration, *Observation of the decay $K^+ \to \pi^+\mu^+\mu^-$*, *Phys. Rev. Lett.* **79** (1997) 4756 [`hep-ex/9708012`] [INSPIRE].

[9] E865 collaboration, *A New measurement of the rare decay $K^+ \to \pi^+\mu^+\mu^-$*, *Phys. Rev. Lett.* **84** (2000) 2580 [`hep-ex/9910047`] [INSPIRE].

[10] HYPERCP collaboration, *Observation of the decay $K^- \to \pi^-\mu^+\mu^-$ and measurements of the branching ratios for $K^\pm \to \pi^\pm\mu^+\mu^-$*, *Phys. Rev. Lett.* **88** (2002) 111801 [`hep-ex/0110033`] [INSPIRE].

[11] NA48/2 collaboration, *New measurement of the $K^\pm \to \pi^\pm\mu^+\mu^-$ decay*, *Phys. Lett. B* **697** (2011) 107 [`arXiv:1011.4817`] [INSPIRE].

[12] P. Bloch et al., *Observation of the $K^+ \to \pi^+e^+e^-$ decay*, *Phys. Lett. B* **56** (1975) 201 [INSPIRE].

[13] C. Alliegro et al., *Study of the decay $K^+ \to \pi^+e^+e^-$*, *Phys. Rev. Lett.* **68** (1992) 278 [INSPIRE].

[14] E865 collaboration, *A New measurement of the properties of the rare decay $K^+ \to \pi + e^+ e^-$*, *Phys. Rev. Lett.* **83** (1999) 4482 [`hep-ex/9907045`] [INSPIRE].

[15] NA48/2 collaboration, *Precise measurement of the $K^\pm \to \pi^\pm e^+ e^-$ decay*, *Phys. Lett. B* **677** (2009) 246 [`arXiv:0903.3130`] [INSPIRE].

[16] G. D'Ambrosio, D. Greynat and M. Knecht, *On the amplitudes for the CP-conserving $K^\pm(K_S) \to \pi^\pm(\pi^0)\ell^+\ell^-$ rare decay modes*, *JHEP* **02** (2019) 049 [`arXiv:1812.00735`] [INSPIRE].

[17] NA62 collaboration, *The beam and detector of the NA62 experiment at CERN*, 2017 *JINST* **12** P05025 [`arXiv:1703.08501`] [INSPIRE].

[18] NA62 collaboration, *Measurement of the very rare $K^+ \to \pi^+ \nu\bar{\nu}$ decay*, *JHEP* **06** (2021) 093 [`arXiv:2103.15389`] [INSPIRE].

[19] R. Ammendola et al., *The integrated low-level trigger and readout system of the CERN NA62 experiment*, *Nucl. Instrum. Meth. A* **929** (2019) 1 [`arXiv:1903.10200`] [INSPIRE].

[20] NA62 collaboration, *Performance of the NA62 trigger system*, `arXiv:2208.00897` [INSPIRE].

[21] J. Allison et al., *Recent developments in Geant4*, *Nucl. Instrum. Meth. A* **835** (2016) 186 [INSPIRE].

[22] PARTICLE DATA GROUP collaboration, *Review of particle physics*, *PTEP* **2022** (2022) 083C01 [INSPIRE].

[23] J. Bijnens and F. Borg, *Isospin breaking in $K \to 3\pi$ decays III: Bremsstrahlung and fit to experiment*, *Eur. Phys. J. C* **40** (2005) 383 [`hep-ph/0501163`] [INSPIRE].

[24] T. Husek, *Standard Model estimate of $K^+ \to \pi^+ 4e$ branching ratio*, *Phys. Rev. D* **106** (2022) L071301 [`arXiv:2207.02234`] [INSPIRE].

[25] G. Isidori, *Soft-photon corrections in multi-body meson decays*, *Eur. Phys. J. C* **53** (2008) 567 [`arXiv:0709.2439`] [INSPIRE].

[26] G. D'Ambrosio, M. Knecht and S. Neshatpour, *Determination of the structure of the $K \to \pi\pi\pi$ amplitudes from recent data*, `arXiv:2209.02143` [INSPIRE].

[27] G.D. Lafferty and T.R. Wyatt, *Where to stick your data points: The treatment of measurements within wide bins*, *Nucl. Instrum. Meth. A* **355** (1995) 541 [INSPIRE].

[28] C.-H. Chen, C.Q. Geng and I.-L. Ho, *Forward backward asymmetry in $K^+ \to \pi^+ \ell^+ \ell^-$*, *Phys. Rev. D* **67** (2003) 074029 [`hep-ph/0302207`] [INSPIRE].

[29] D.-N. Gao, *Long distance contribution to the forward backward asymmetry in decays $K^+ \to \pi^+ \ell^+ \ell^-$*, *Phys. Rev. D* **69** (2004) 094030 [`hep-ph/0311253`] [INSPIRE].

[30] NA62 collaboration, *Searches for lepton number violating K^+ decays*, *Phys. Lett. B* **797** (2019) 134794 [`arXiv:1905.07770`] [INSPIRE].

[31] PARTICLE DATA GROUP collaboration, *Review of particle physics*, *J. Phys. G* **37** (2010) 075021 [INSPIRE].

The NA62 collaboration

E. Cortina Gil,[1] A. Kleimenova,[1,a] E. Minucci,[1,b,c] S. Padolski,[1,d] P. Petrov,[1] A. Shaikhiev,[1,e]
R. Volpe,[1,f] T. Numao,[2] Y. Petrov,[2] B. Velghe,[2] V.W.S. Wong,[2] D. Bryman,[3,g] J. Fu,[3]
T. Husek,[4,h] J. Jerhot,[4,i] K. Kampf,[4] M. Zamkovsky,[4,b] R. Aliberti,[5,j] G. Khoriauli,[5,k]
J. Kunze,[5] D. Lomidze,[5,l] L. Peruzzo,[5] M. Vormstein,[5] R. Wanke,[5] P. Dalpiaz,[6] M. Fiorini,[6]
I. Neri,[6] A. Norton,[6,m] F. Petrucci,[6] H. Wahl,[6,n] A. Cotta Ramusino,[7] A. Gianoli,[7]
E. Iacopini,[8] G. Latino,[8] M. Lenti,[8] A. Parenti,[8] A. Bizzeti,[9,o] F. Bucci,[9] A. Antonelli,[10]
G. Georgiev,[10,p] V. Kozhuharov,[10,p] G. Lanfranchi,[10] S. Martellotti,[10] M. Moulson,[10]
T. Spadaro,[10] G. Tinti,[10] F. Ambrosino,[11] T. Capussela,[11] M. Corvino,[11,b] D. Di Filippo,[11]
R. Fiorenza,[11,q] P. Massarotti,[11] M. Mirra,[11] M. Napolitano,[11] G. Saracino,[11] G. Anzivino,[12]
F. Brizioli,[12,b] E. Imbergamo,[12] R. Lollini,[12] R. Piandani,[12,r] C. Santoni,[12] M. Barbanera,[13]
P. Cenci,[13] B. Checcucci,[13] P. Lubrano,[13] M. Lupi,[13,s] M. Pepe,[13] M. Piccini,[13]
F. Costantini,[14] L. Di Lella,[14,n] N. Doble,[14,n] M. Giorgi,[14] S. Giudici,[14] G. Lamanna,[14]
E. Lari,[14] E. Pedreschi,[14] M. Sozzi,[14] C. Cerri,[15] R. Fantechi,[15] L. Pontisso,[15,t] F. Spinella,[15]
I. Mannelli,[16] G. D'Agostini,[17] M. Raggi,[17] A. Biagioni,[18] P. Cretaro,[18] O. Frezza,[18]
E. Leonardi,[18] A. Lonardo,[18] M. Turisini,[18] P. Valente,[18] P. Vicini,[18] R. Ammendola,[19]
V. Bonaiuto,[19,u] A. Fucci,[19] A. Salamon,[19] F. Sargeni,[19,v] R. Arcidiacono,[20,w]
B. Bloch-Devaux,[20] M. Boretto,[20,b] E. Menichetti,[20] E. Migliore,[20] D. Soldi,[20] C. Biino,[21]
A. Filippi,[21] F. Marchetto,[21] J. Engelfried,[22] N. Estrada-Tristan,[22,x] A.M. Bragadireanu,[23]
S.A. Ghinescu,[23] O.E. Hutanu,[23] A. Baeva,[24] D. Baigarashev,[24,y] D. Emelyanov,[24] T. Enik,[24]
V. Falaleev,[24,z] V. Kekelidze,[24] A. Korotkova,[24] L. Litov,[24,p] D. Madigozhin,[24]
M. Misheva,[24,aa] N. Molokanova,[24] S. Movchan,[24] I. Polenkevich,[24] Yu. Potrebenikov,[24]
S. Shkarovskiy,[24] A. Zinchenko,[24,†] S. Fedotov,[25] E. Gushchin,[25] A. Khotyantsev,[25]
Y. Kudenko,[25,ab] V. Kurochka,[25] M. Medvedeva,[25] A. Mefodev ,[25] S. Kholodenko,[26]
V. Kurshetsov,[26] V. Obraztsov,[26] A. Ostankov,[26,†] V. Semenov,[26,†] V. Sugonyaev,[26]
O. Yushchenko,[26] L. Bician,[27,ac,*] T. Blazek,[27] V. Cerny,[27] Z. Kucerova,[27] J. Bernhard,[28]
A. Ceccucci,[28] H. Danielsson,[28] N. De Simone,[28,ad] F. Duval,[28] B. Döbrich,[28] L. Federici,[28]
E. Gamberini,[28] L. Gatignon,[28,ae] R. Guida,[28] F. Hahn,[28,†] E.B. Holzer,[28] B. Jenninger,[28]
M. Koval,[28,ac] P. Laycock,[28,d] G. Lehmann Miotto,[28] P. Lichard,[28] A. Mapelli,[28]
R. Marchevski,[28,af] K. Massri,[28] M. Noy,[28] V. Palladino,[28] M. Perrin-Terrin,[28,ag,ah]
J. Pinzino,[28,ai] V. Ryjov,[28] S. Schuchmann,[28] S. Venditti,[28] T. Bache,[29] M.B. Brunetti,[29,aj]
V. Duk,[29,f] V. Fascianelli,[29,ak] J. R. Fry,[29] F. Gonnella,[29] E. Goudzovski,[29] J. Henshaw,[29]
L. Iacobuzio,[29] C. Lazzeroni,[29] N. Lurkin,[29,i] F. Newson,[29] C. Parkinson,[29] A. Romano,[29]
A. Sergi,[29,al] A. Sturgess,[29] J. Swallow,[29,b] A. Tomczak,[29] H. Heath,[30] R. Page,[30] S. Trilov,[30]
B. Angelucci,[31] D. Britton,[31] C. Graham,[31] D. Protopopescu,[31] J. Carmignani,[32,am]
J.B. Dainton,[32] R.W. L. Jones,[32] G. Ruggiero,[32,an] L. Fulton,[33] D. Hutchcroft,[33]
E. Maurice,[33,ao] B. Wrona,[33] A. Conovaloff,[34] P. Cooper,[34] D. Coward,[34,ap] and P. Rubin[34]

[1] *Université Catholique de Louvain, B-1348 Louvain-La-Neuve, Belgium*

[2] *TRIUMF, Vancouver, British Columbia, V6T 2A3, Canada*

[3] *University of British Columbia, Vancouver, British Columbia, V6T 1Z4, Canada*

[4] *Charles University, 116 36 Prague 1, Czech Republic*

[5] *Institut für Physik and PRISMA Cluster of Excellence, Universität Mainz, D-55099 Mainz, Germany*

[6] *Dipartimento di Fisica e Scienze della Terra dell'Università e INFN, Sezione di Ferrara, I-44122 Ferrara, Italy*

[7] *INFN, Sezione di Ferrara, I-44122 Ferrara, Italy*

[8] *Dipartimento di Fisica e Astronomia dell'Università e INFN, Sezione di Firenze, I-50019 Sesto Fiorentino, Italy*

9 *INFN, Sezione di Firenze, I-50019 Sesto Fiorentino, Italy*

10 *Laboratori Nazionali di Frascati, I-00044 Frascati, Italy*

11 *Dipartimento di Fisica "Ettore Pancini" e INFN, Sezione di Napoli, I-80126 Napoli, Italy*

12 *Dipartimento di Fisica e Geologia dell'Università e INFN, Sezione di Perugia, I-06100 Perugia, Italy*

13 *INFN, Sezione di Perugia, I-06100 Perugia, Italy*

14 *Dipartimento di Fisica dell'Università e INFN, Sezione di Pisa, I-56100 Pisa, Italy*

15 *INFN, Sezione di Pisa, I-56100 Pisa, Italy*

16 *Scuola Normale Superiore e INFN, Sezione di Pisa, I-56100 Pisa, Italy*

17 *Dipartimento di Fisica, Sapienza Università di Roma e INFN, Sezione di Roma I, I-00185 Roma, Italy*

18 *INFN, Sezione di Roma I, I-00185 Roma, Italy*

19 *INFN, Sezione di Roma Tor Vergata, I-00133 Roma, Italy*

20 *Dipartimento di Fisica dell'Università e INFN, Sezione di Torino, I-10125 Torino, Italy*

21 *INFN, Sezione di Torino, I-10125 Torino, Italy*

22 *Instituto de Física, Universidad Autónoma de San Luis Potosí, 78240 San Luis Potosí, Mexico*

23 *Horia Hulubei National Institute for R&D in Physics and Nuclear Engineering, 077125 Bucharest-Magurele, Romania*

24 *Joint Institute for Nuclear Research, 141980 Dubna (MO), Russia*

25 *Institute for Nuclear Research of the Russian Academy of Sciences, 117312 Moscow, Russia*

26 *Institute for High Energy Physics of the Russian Federation, State Research Center "Kurchatov Institute", 142281 Protvino (MO), Russia*

27 *Faculty of Mathematics, Physics and Informatics, Comenius University, 842 48, Bratislava, Slovakia*

28 *CERN, European Organization for Nuclear Research, CH-1211 Geneva 23, Switzerland*

29 *School of Physics and Astronomy, University of Birmingham, Edgbaston, Birmingham, B15 2TT, U.K.*

30 *School of Physics, University of Bristol, Bristol, BS8 1TH, U.K.*

31 *School of Physics and Astronomy, University of Glasgow, Glasgow, G12 8QQ, U.K.*

32 *Faculty of Science and Technology, University of Lancaster, Lancaster, LA1 4YW, U.K.*

33 *School of Physical Sciences, University of Liverpool, Liverpool, L69 7ZE, U.K.*

34 *Physics and Astronomy Department, George Mason University, Fairfax, VA 22030, U.S.A.*

* *Corresponding author*

† *Deceased*

a *Present address: Faculty of Mathematics, Physics and Informatics, Comenius University, 842 48, Bratislava, Slovakia*

b *Present address: CERN, European Organization for Nuclear Research, CH-1211 Geneva 23, Switzerland*

c *Also at Laboratori Nazionali di Frascati, I-00044 Frascati, Italy*

d *Present address: Brookhaven National Laboratory, Upton, NY 11973, U.S.A.*

e *Present address: School of Physics and Astronomy, University of Birmingham, Birmingham, B15 2TT, U.K.*

f *Present address: INFN, Sezione di Perugia, I-06100 Perugia, Italy*

g *Also at TRIUMF, Vancouver, British Columbia, V6T 2A3, Canada*

h *Present address: Department of Astronomy and Theoretical Physics, Lund University, Lund, SE 223-62, Sweden*

i *Present address: Université Catholique de Louvain, B-1348 Louvain-La-Neuve, Belgium*

j *Present address: Institut für Kernphysik and Helmholtz Institute Mainz, Universität Mainz, Mainz, D-55099, Germany*

k *Present address: Universität Würzburg, D-97070 Würzburg, Germany*

l *Present address: European XFEL GmbH, D-22761 Hamburg, Germany*

m *Present address: School of Physics and Astronomy, University of Glasgow, Glasgow, G12 8QQ, U.K.*

^{n} Present address: Institut für Physik and PRISMA Cluster of Excellence, Universität Mainz, D-55099 Mainz, Germany

^{o} Also at Dipartimento di Scienze Fisiche, Informatiche e Matematiche, Università di Modena e Reggio Emilia, I-41125 Modena, Italy

^{p} Also at Faculty of Physics, University of Sofia, BG-1164 Sofia, Bulgaria

^{q} Present address: Scuola Superiore Meridionale e INFN, Sezione di Napoli, I-80138 Napoli, Italy

^{r} Present address: Instituto de Física, Universidad Autónoma de San Luis Potosí, 78240 San Luis Potosí, Mexico

^{s} Present address: Institut am Fachbereich Informatik und Mathematik, Goethe Universität, D-60323 Frankfurt am Main, Germany

^{t} Present address: INFN, Sezione di Roma I, I-00185 Roma, Italy

^{u} Also at Department of Industrial Engineering, University of Roma Tor Vergata, I-00173 Roma, Italy

^{v} Also at Department of Electronic Engineering, University of Roma Tor Vergata, I-00173 Roma, Italy

^{w} Also at Università degli Studi del Piemonte Orientale, I-13100 Vercelli, Italy

^{x} Also at Universidad de Guanajuato, 36000 Guanajuato, Mexico

^{y} Also at L.N. Gumilyov Eurasian National University, 010000 Nur-Sultan, Kazakhstan

^{z} Also at Institute for Nuclear Research of the Russian Academy of Sciences, 117312 Moscow, Russia

^{aa} Present address: Institute of Nuclear Research and Nuclear Energy of Bulgarian Academy of Science (INRNE-BAS), BG-1784 Sofia, Bulgaria

^{ab} Also at National Research Nuclear University (MEPhI), 115409 Moscow and Moscow Institute of Physics and Technology, 141701 Moscow region, Moscow, Russia

^{ac} Present address: Charles University, 116 36 Prague 1, Czech Republic

^{ad} Present address: DESY, D-15738 Zeuthen, Germany

^{ae} Present address: Faculty of Science and Technology, University of Lancaster, Lancaster, LA1 4YW, U.K.

^{af} Present address: Weizmann Institute, Rehovot, 76100, Israel

^{ag} Present address: Aix Marseille University, CNRS/IN2P3, CPPM, F-13288, Marseille, France

^{ah} Also at Université Catholique de Louvain, B-1348 Louvain-La-Neuve, Belgium

^{ai} Present address: INFN, Sezione di Pisa, I-56100 Pisa, Italy

^{aj} Present address: Department of Physics, University of Warwick, Coventry, CV4 7AL, U.K.

^{ak} Present address: Center for theoretical neuroscience, Columbia University, New York, NY 10027, U.S.A.

^{al} Present address: Dipartimento di Fisica dell'Università e INFN, Sezione di Genova, I-16146 Genova, Italy

^{am} Present address: School of Physical Sciences, University of Liverpool, Liverpool, L69 7ZE, U.K.

^{an} Present address: Dipartimento di Fisica e Astronomia dell'Università e INFN, Sezione di Firenze, I-50019 Sesto Fiorentino, Italy

^{ao} Present address: Laboratoire Leprince Ringuet, F-91120 Palaiseau, France

^{ap} Also at SLAC National Accelerator Laboratory, Stanford University, Menlo Park, CA 94025, U.S.A.